2008–2009

Use of MODIS imagery for the assessment of the variability in intertidal microphytobenthos biomass at regional and global scales.

by
Quinten Vanhellemont

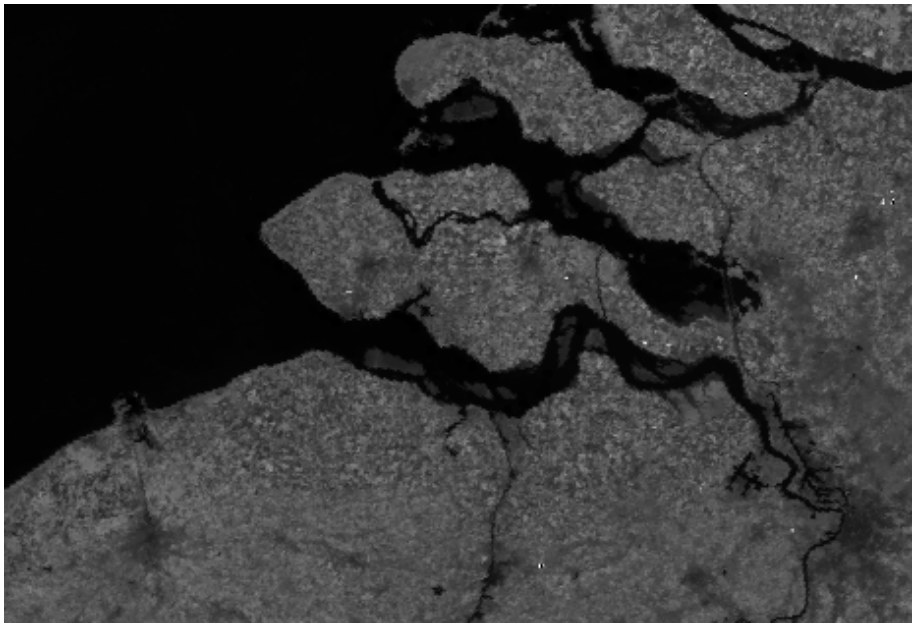

Promoter: Koen Sabbe
Co-promoter: Rudi Goossens
Daphne Van der Wal
Mentor: Aaike De Wever

Thesis submitted to obtain the degree of Master in Marine and Lacustrine Sciences (Faculty of Science)

MareLac – Masters Science Degree Course – Ghent University
Advanced Studies in Marine and Lacustrine Sciences

Abstract

Using remote sensing data, we studied large scale patterns in spatial and seasonal dynamics of microphytobenthos biomass on intertidal areas along latitudinal gradients. To this aim, we calculated the Normalized Difference Vegetation Index (NDVI) using coarse resolution (250 m) data from the Moderate Resolution Imaging Spectroradiometer (MODIS) for twelve intertidal areas around the world. Our results for two well-studied areas, the Western Scheldt estuary and the Mont Saint-Michel bay, show that MODIS data are suitable for assessing spatial and temporal dynamics of intertidal microphytobenthos on large mudflats (> 50 km^2). Our results show that the average annual microphytobenthos biomass increases from the equator to the poles. Higher latitude (i.e. temperate) sites also have more pronounced seasonal patterns, usually with significantly higher biomass during the warmer spring and summer months. Within the mudflats, there is a strong positive relationship between elevation and microphytobenthos biomass. Although we observed large differences between sites on different latitudes, a large within-site variability remained. Some mudflats deviated from the general pattern we observed. However, for most study areas a detailed interpretation of the images is not yet possible, as no data on microphytobenthos, or even sediment and vegetation are available. In conclusion, MODIS imagery appears to be very suitable for the assessment of global to regional large-scale patterns in microphytobenthos biomass.

Keywords

Microphytobenthos · Biomass · Intertidal mudflat · Seasonal dynamics · NDVI · Remote sensing

1 Introduction

The intertidal zone is located at the interface of the terrestrial, marine and atmospheric environment and is periodically covered and uncovered by the sea. A variety of habitats can exist in this zone, mainly determined by local characteristics; Intertidal mudflats only occur in regions with abundant soft sediments, often in combination with a relatively large tidal range. The typically unstable sediments and fluctuating conditions of these flats are unfavourable to most macrophytes, but allow benthic microphytes to thrive (Admiraal, 1984). Microphytobenthos account for a large part of the primary production on intertidal flats (Blanchard et al., 1998; Underwood and Kromkamp, 1999), and is generally dominated by diatoms (Admiraal, 1984; Paterson et al., 1998). Cyanobacteria and flagellates are more important in the tropics (MacIntyre et al., 1996). Because of their high productivity, intertidal mudflats are excellent foraging and over-wintering areas for birds as well as nursery grounds for fish (Baeyens et al., 1998).

When the mudflats are exposed to light at low tide, motile microphytobenthos (i.e. epipelon) migrates to the top sediment layer, resulting in the formation of dense algal mats (Underwood and Kromkamp, 1999; Decho, 2000). The presence of algal mats, or biofilms, varies greatly on both temporal and spatial scales, which makes the assessment of their primary production, biomass or distribution difficult (Shaffer and Onuf, 1985; Paterson et al., 1998; Seuront and Leterme, 2006). Microphyhobenthos excrete Extracellular Polymeric Substances (EPS) that typically increase the sediment stability and thus decrease the erosion on mudflats (Miller et al., 1996; Tolhurst et al., 1999; Smith et al., 2003). EPS can be produced by the migration mechanisms of the microphytobenthos (Smith and Underwood, 1998), or can be excreted during periods of high photosynthesis during nutrient limitation (Underwood, 2002). Temperature and light probably have the largest effects on benthic primary production (MacIntyre et al., 1996). These two variables vary under the influence of a wide range of factors, ranging from global factors such as latitude and climate, to regional and local factors, such as exposure time and weather (Admiraal, 1984; Blanchard et al., 1997). In addition, the time of exposure determines the temperature and insolation patterns on the mudflat. The short-term dynamics – a few hours to a fortnight – of the microphytobenthos are mainly determined by the tidal cycle (Blanchard et al., 1998), and are largely affected by the migratory behavior of the epipelon (Serôdio et al., 2001).

Microphytobenthos dynamics are also greatly influenced by other factors such as sediment composition, elevation, and grazing. The sediment composition is a key factor in determining microphytobenthos biomass. In cohesive, muddy sediments,

the microphytobenthos is dominated by epipelic diatoms while in less cohesive, sandy sediments non-motile (i.e. epipsammic) species are more frequent (Yallop et al., 1994). Light penetration is lower in cohesive muddy sediments (ca. 0.5 mm) than in non-cohesive sandy sediments (ca. 2 mm), which might explain the success of motile species in muddy sediments (Yallop et al., 1994; Paterson and Hagerthey, 2001). On cohesive sediments, biomass tends to be higher than on non-cohesive sediments because of higher nutrient concentrations, smaller particle sizes, and less frequent disturbances (Underwood and Kromkamp, 1999; Paterson and Hagerthey, 2001). A higher microphytobenthos biomass can generally be found towards higher elevations in dynamic and turbid systems (de Jong and de Jonge, 1995). In calmer systems, the water transparency remains high, which allows light to penetrate to the sediment layer during high tide, and no clear link can be found between microphytobenthos biomass and elevation (Stapel and de Jong, 1998). The lower shores have a limited light availability, which in combination with frequent disturbances prevents the buildup of microphytobenthos biomass (Underwood and Kromkamp, 1999). On higher shores, however, the microphytobenthos is subject to higher rates of desiccation, higher temperatures and increased incident sunlight. Microphytobenthos is of crucial importance in the carbon flow in coastal sediments (Middelburg et al., 2000), and is a very important food source for benthic herbivores (Nicotri, 1977; Blanchard et al., 1998; Ford and Honeywill, 2002; Hagerthey et al., 2002).

An increase of microphytobenthos biomass during late spring and early summer has been found in many studies on intertidal mudflats, yet other studies found no significant seasonal patterns (MacIntyre et al., 1996). According to Cadée and Hegeman (1974) [cited in Underwood and Kromkamp (1999)], microphytobenthos is less affected by seasonality than phytoplankton. This indicates that not only latitude, but also mudflat-specific characteristics have a rather important impact on the seasonal dynamics of microphytobenthos. The generalized observation of a maximum biomass during spring and summer is also very likely biased, as most microphytobenthos studies have been performed in Europe and North America, for which Cahoon (2006) lists evident reasons such as funding, logistics and local relevance.

The sampling of previous studies has been rather limited in space and time. Therefore the application of remote sensing on intertidal flats has recently gained interest, as it allows the observation of extensive and inaccessible areas over a long period of time. On average, most long-term studies on microphytobenthos variability have a duration of one to two years, e.g. studies by de Jong and de Jonge (1995); Thornton et al. (2002); Montani et al. (2003); Migné et al. (2004); Méléder

et al. (2005); Koh et al. (2007). This illustrates the high potential value of large archives with remotely sensed data from several years. Especially remotely sensed data with a high temporal resolution could prove to be very useful for the research on intertidal flats. These data can provide valuable information on the large-scale ecological patterns of these systems, both in space and time. Most studies of intertidal flats using remote sensing data have used a combination of field spectrometry and airborne sensors (Combe et al., 2005; Deronde et al., 2006). The resolution of airborne sensors is superior to that of space-borne sensors (around one to two metres), and the data collection using airborne sensors can be timed to coincide with low tide. However, airborne sensors are very expensive to deploy. Field spectrometry is very time consuming, and since this method samples discrete points, a complete coverage of the intertidal mudflat is hard to attain. Space-borne sensors have been used less frequently, for example by Méléder et al. (2003). The spatial and temporal resolution of a space-borne sensor are strongly linked. A sensor with a high spatial resolution, and thus a small swath width, automatically has a longer time between repeated captures of the same area, and vice versa. Studies using space-borne remote sensing have focused on data from higher resolution hyperspectral sensors, with a ground resolution from a few to a few tens of metres. The cost of the high-resolution imagery and the low recurrence time has probably limited the use to a few images. As a result, no real time series of remotely sensed data have been collected for intertidal areas, and the high-resolution space-borne imagery gained a more supportive role in the research. Due to their larger swath width, space-borne sensors with a relatively coarse ground resolution (a few hundreds of metres) can yield a better temporal resolution. For example, the Moderate Resolution Imaging Spectroradiometer (MODIS) on the Aqua satellite could in theory capture the same area at a daily frequency. Sensors with a large spatial resolution, such as MODIS, are less suitable for determination of microphytobenthos biomass, although the large scale patterns are retained (der Wal, 2008). However, MODIS data have not yet been widely used on intertidal areas except for recent work by Van der Wal (*unpubl.*).

The aim of our study is to evaluate whether coarse resolution (250 m) space-borne remote-sensed data from MODIS can be used to assess the spatial and seasonal dynamics of microphytobenthos in large intertidal areas, i.e. from twenty to several hundreds of km^2, along latitudinal gradients. The study we present is the first to analyze and summarize the large-scale patterns in several intertidal areas using remotely sensed data. The suitability as a proxy for microphytobenthos biomass of the Normalized Difference Vegetation Index (NDVI) calculated using MODIS data was evaluated for two study areas, for which information on microphytobenthos biomass and environmental variables was available (the West-

ern Scheldt estuary and the Mont Saint-Michel bay). Subsequently, ten additional areas were selected along a latitudinal gradient to study the latitudinal variation in biomass and the dynamics of the microphytobenthos. MODIS Aqua data was obtained and processed for the twelve study areas for the year 2003.

2 Methods

2.1 Study Area

Based on literature and other information on intertidal mudflats, such as personal observations and areas found on Google Earth, suitable study sites were selected along a latitudinal gradient. The NDVI, a widely applicable index for plant vegetation in general, was used as a proxy for microphytobenthic biomass. Therefore, the study sites have to be dominated by microphytobenthos, rather than by sea-grasses, macro-algae, salt-marsh or mangrove vegetation. Due to the limited ground resolution of the used MODIS bands (see below), which is about 250 m, the intertidal flats have to be at least several square kilometres in size. We selected sixty areas of which twelve were retained for further study (see Fig. 1 and Table 1), based on the position along the latitudinal gradient and the amount of information directly available. Little information is available on the community composition of primary producers on mudflats in developing countries, the dominance of microphytobenthos or the presence of salt-marshes for example is not described in scientific literature. In some cases, even tidal ranges and recent climate data are not readily available. Therefore, most study areas are situated in developed countries, where this information is more easily obtained. The site codes in the first column of Table 1 will be used to refer to the study areas.

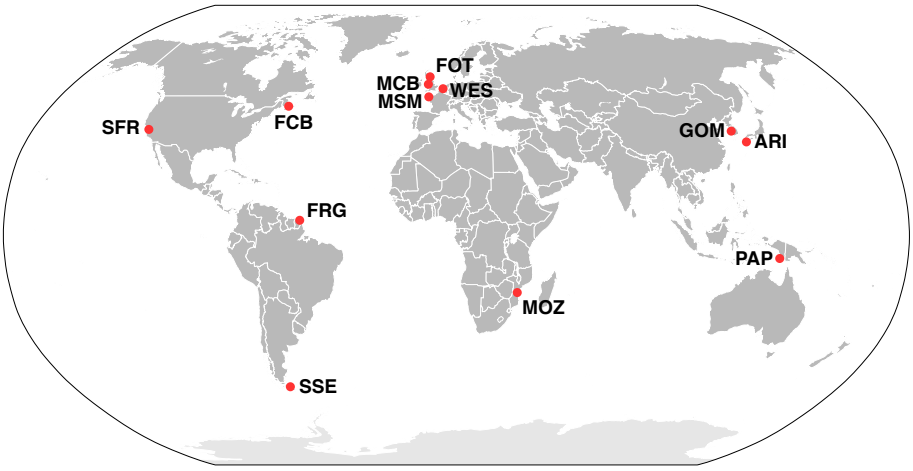

Figure 1: Geographical position of the study areas. For an overview of the areas, see Table 1. Base map obtained from Wikipedia (http://en.wikipedia.org/)

Table 1: The twelve study areas sorted according to latitude (N-S); the dashed line indicates the position of the equator. Countries are represented with the three-character ISO 3166-1 standard. The latitude and longitude indicate the central point of the region of interest. References refer to published literature which includes information on the environment and/or the microphytobenthos of the study area. The number of images used in the analysis is given with the total number of images obtained between brackets. The tides are represented either by mean (m) or spring (s) tidal ranges (in metre). Mudflat extent in (km^2) is based on the maximum observed number of pixels (between brackets).

Code	Area (Country)	Location	Reference	Images	Tides	Extent
FOT	Firth of Tay (GBR)	56°25'N 3°6'W	Bates et al. (2004)	28(49)	5(s)	37(595)
MCB	Morecambe Bay (GBR)	54°5'N 2°58'W	Mason et al. (1999)	52(78)	8(s)	246(3943)
WES	Western Scheldt estuary (NLD)	51°24'N 3°53'E	de Jong and de Jonge (1995) Forster et al. (2006)	51(64)	5(m)	55(879)
MSM	Mont Saint-Michel Bay (FRA)	48°40'N 1°38'W	Riera (2007)	58(69)	12(s)	155(2478)
FCB	Chignecto Bay (CAN)	45°48'N 64°29'W	Trites et al. (2005)	36(94)	11(m)	45(718)
SFR	South San Francisco Bay (USA)	37°30'N 122°6'W	Guarini et al. (2002)	33(83)	2(m)	20(325)
GOM	Gomso Bay (KOR)	35°34'N 126°33'E	Oh and Koh (1995) Ryu et al. (2008)	42(63)	4.5(m)	48(771)
ARI	Ariake Sea (JPN)	33°6'N 130°16'E	Koh et al. (2007)	27(53)	5.5(s)	63(1003)
FRG	French Guyana Mudflats (GUF)	5°31'N 53°10'W	Fiot and Gratiot (2006)	63(85)	2(m)	227(3623)
PAP	Frederik Hendrik Island (IDN)	7°42'S 138°5'E	no reference	15(48)	–	402(6433)
MOZ	Mudflats South of Beira (MOZ)	20°24'S 34°45'E	Deppe (2000)	46(92)	6.5(s)	94(1497)
SSE	San Sebastian Bay (ARG)	53°10'S 68°25'W	Vilas et al. (1999)	58(78)	10(s)	118(1887)

2.2 NDVI Calculation

We used the Normalized Difference Vegetation Index (NDVI) as a proxy for microphytobenthos biomass. For terrestrial vegetation, the MODIS NDVI is sensitive to seasonal vegetation variations, and has a good dynamic range in the detection of vegetation amount and condition (Huete et al., 2002). The data were analyzed using R version 2.8.0 (http://www.r-project.org/), a free and open software environment for statistical analysis. The NDVI was calculated for each pixel of each image. The NDVI is defined as (King et al., 1992)

$$\frac{NIR - RED}{NIR + RED}. \tag{1}$$

NIR and RED are the reflectance values in the near-infrared and red band, i.e. band 1 (620–670 nm) and band 2 (841–876 nm) for MODIS. NDVI values always range from -1 to +1, where 0 represents no vegetation. Vegetated areas will produce a positive NDVI value because vegetation has a high reflectance in near-infrared, and a low reflectance in red. Clouds, water and ice will generate a negative NDVI, because they have a large visible reflectance, and a lower reflectance in the near-infrared (Lillesand and Kiefer, 2000, p. 448). Because the NDVI mainly is sensitive to variations in the red band, a saturation of the NDVI is easily reached for areas with large amounts of vegetation (Pettorelli et al., 2005). For terrestrial vegetation, the upper limit of the MODIS NDVI is about 0.9, with saturation effects starting around 0.7 (Huete et al., 2002). For microphytobenthos on intertidal areas, Méléder et al. (2003) found a saturation of the NDVI at around 0.4, and suggested that it should only be used for the assessment of low biomass concentrations. However, they calculated the NDVI with simulated SPOT bands based data from field spectrometry. SPOT bands have a somewhat wider spectral range than MODIS bands. In general, NDVI values from different sensors are not equivalent, as bandwidth and sensitivity can differ between sensors (Steven et al., 2006). A correction could be applied to our NDVI, but this was not within the scope of this research. Due to the combination of the patchiness in microphytobenthos biomass distribution (Seuront and Leterme, 2006) and the coarse ground resolution of MODIS, such high NDVI values were not observed. Because the NDVI is ratio-based, a drawback inherent to the use of the NDVI is the amplification of additive noise, e.g. caused by atmospheric effects. An advantage of the NDVI is the reduction of multiplicative noise, such as illumination and atmospheric attenuation differences (Huete et al., 2002).

2.3 Image Selection

It was decided early on to use images from 2003, since Van der Wal (*pers. comm.*) obtained good results for the Scheldt estuary and the Wadden Sea with MODIS data from 2003. In Europe, the summer of 2003 was characterized by an exceptionally high number of sunshine hours, as well as by high temperatures and very low precipitation (Rebetez et al., 2006). In addition, as the MODIS Aqua instrument was launched in 2002, quality drawbacks inherent to an ageing sensor were avoided. Since the applications for MODIS data are so varied, data can be obtained in a very large number of different formats. For the purposes of this research, the images have to include both the red and near-infrared high-resolution bands in order to calculate the NDVI. Besides, the images have to include data from only one day to ensure a temporal resolution as high as possible.

Initially, we obtained unprocessed Level 0 (L0) MODIS images from the OceanColor website (http://oceancolor.gsfc.nasa.gov/). These images contain low-level data for all thirty-six MODIS bands. Processing to L1B and the extraction of the 250 m bands (bands 1 and 2) was done in OceanColor's own SeaDAS (http://oceancolor.gsfc.nasa.gov/seadas/). Georeferencing and removal of the bow-tie effect on L1B images did not deliver adequate results. On the resulting images, pixels could not be perfectly matched between images from the same area. This introduced difficulties in comparing the images, e.g. the application of the same region of interest, and rendered pixel-per-pixel comparison impossible. Daily, monthly and seasonal NDVI maps based on these images would not be comparable, or even impossible to create. As the problems of using these images became apparent, it was decided to use L2G images from the Land Processes Distributed Active Archive Center (LPDAAC) instead. The L2G images only contain the first two bands and do not require processing apart from a format conversion. These images originate from the "Surface Reflectance Daily L2G Global 250 m" dataset, with internal identification MYD09GQ. These L2G images provide estimates for surface reflectance in the first two MODIS bands. The data are stored using the sinusoidal projection, which is an equal area projection that distorts shapes and directions. The latter is actually an advantage for this research, as we are not really interested in the true shape of the intertidal areas, and it makes comparing sizes between areas possible. A disadvantage of these images is that it is not clearly documented at what time each pixel was captured, as L2G images are a composite of several adjacent overpasses, which can be spaced up to a few hours apart.

For each of the selected sites in Table 1, L2G MODIS Aqua images were obtained using the Warehouse Inventory Search Tool (WIST). A minor drawback of WIST is the absence of quicklook images, i.e. small versions of the full scenes, which are useful to determine whether or not to download an image. Bandwidth, disk space and processing time are greatly reduced when images are excluded on which clouds cover the area of interest. This limitation of WIST was avoided by using the quicklook images provided by the OceanColor search tool. The number of downloaded images (between brackets) and the final number of images used in the analysis is included in Table 1. The theoretical maximum of 365 images per year for each study area is sharply reduced because of cloud cover on the quicklooks. A second reduction occurred after downloading and processing (see below). The decrease in usable images for MSM is lower than for the rest of the areas, because the image capture times were checked for tidal height before downloading. This time-consuming check-up was abandoned after it became apparent that the tidal exposure can be determined from the images themselves (cfr. 2.4.4). The higher fraction of retained images for WES is a result of the fact that this is an extensive

estuarine system with large spatial differences in the tidal cycle along the estuarine axis, which increases the chance that some parts of the mudflats are exposed.

2.4 Quality control and data processing

2.4.1 Image conversion and ROI definition

A conversion from the hierarchical data format (.hdf) to the more conventional geotiff format (.tif) is necessary in order to use the L2G images in ITT ENVI (http://www.ittvis.com/ENVI/). Note that no additional resampling took place during this conversion step. After image acquisition and conversion, a first quality check was performed on the converted images to exclude unusable images, e.g. distorted images, images with cloud cover (which was not visible on the quicklook images) or images taken during high tide. The extent of bare mudflat was used as a proxy for tidal height at the moment of capture (see 2.4.4). A region of interest (ROI) was determined for each area, using the best high and low tide images. Based on the second band (NIR) of the selected high- and low-tide images, the ROI was hand-drawn with the ROI tool in ITT ENVI. Special attention was paid to the landward side of the ROI, in order not to include pixels with terrestrial vegetation. The seaward side of the ROI was drawn more flexibly, as these redundant 'sea pixels' could be excluded automatically (see further). The data of the ROI were subsequently exported to an ASCII file for both bands of each image, necessary to calculate the NDVI.

2.4.2 Band Thresholds

After the first images were processed, it became clear that an additional threshold had to be put on the band values. On some images, a number of NDVI values larger than 1 were observed, values which are impossible (see Eq. 1), since by definition reflectance is a positive real number. These large NDVI values are caused by the fact that reflectance values in the MYD09QG data set ranges from -100 to 16000. Additionally, it appears that the near-infrared band does not perform well at low reflectance values, which results in unrealistically high positive NDVI values (> 0.6) – some even larger than the values observed above dense tropical forest canopies (Huete et al., 2002). This effect mostly occurs in water pixels, where the reflectance is low in both red and near-infrared bands. In combination with a faulty atmospheric correction this creates these very large NDVI values. In order to avoid these unrealistic NDVI values, the effect of lower thresholds on the MODIS bands prior to NDVI calculation was tested (0 for the red band, and thresholds of 0, 20, 200, 320 and 500 for the near-infrared band). The use of reflectance thresholds of at least 0 in the red band and at least 320 in the near-infrared bands, similar to

the thresholds used by Van der Wal (*pers. comm.*), proved to be very effective in removing the erroneous values while retaining valuable 'true' values (see Figure 2). NDVI values were recalculated after applying these thresholds to the data.

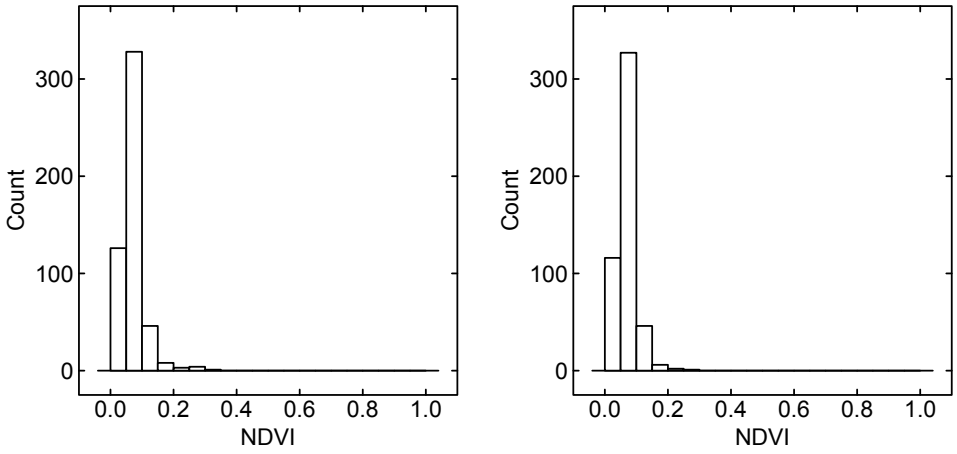

(a) 25 May 2003, before (0.0719)

(b) 25 May 2003, after (0.0705)

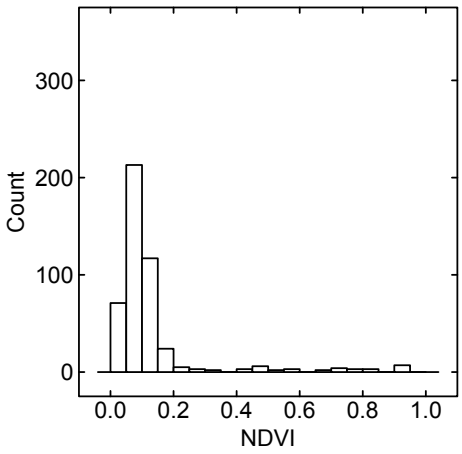

(c) 19 August 2003, before (0.1301)

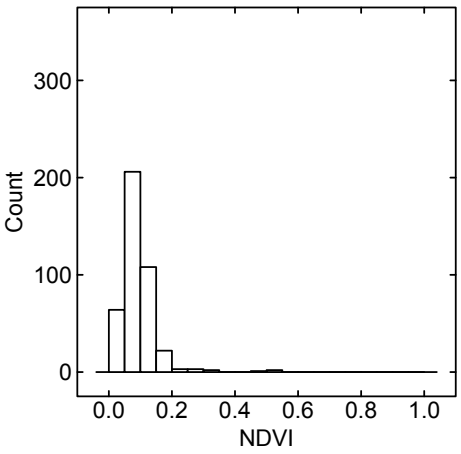

(d) 19 August 2003, after (0.0907)

Figure 2: Histograms of the NDVI values on the Mont Saint-Michel Bay mudflat, before and after application of the boundary on the near-infrared band for a typical image [25 May 2003, (a) and (b)] and an image with unrealistically high (> 0.6) NDVI values [19 August 2003, (c) and (d)]. Mean NDVI values between brackets. Note that the images already passed a filter to exclude negative reflectance values on both bands.

2.4.3 Removal of sea pixels

Because a pixel with negative NDVI either represents water, ice or clouds (see 2.2), we omitted NDVI values smaller than 0, thus excluding these pixels from the data set. After processing, however, it appeared that a couple of images per area had unrealistically positive NDVI values in the adjacent waters. These values can be considered erroneous, as they are caused by a larger reflectance in the near-infrared band, probably due to the high turbidity of the near-shore waters (Ruddick et al., 2000; Siegel et al., 2000), or due to effects that were not removed after applying the band thresholds (see 2.4.2). As this pattern was quite random for each image, we omitted pixels that occurred only on one or two images per area for the 2003 dataset (the "three image criterion"). This procedure was tested on the MCB data set, where some images showed a clear group of erroneous pixels in the adjacent water area. A strong reduction of these erroneous 'sea pixels' is obtained using the three image criterion, while true mudflat pixels remain unaffected (Fig. 3). A reduction of erroneous values present in the area that is exposed mudflat on other images was not possible using the three image criterion. For example, the very low NDVI values in the lower centre and in the centre-right of Fig. 3b cannot be removed. Because the erroneous pixels generally have a very low NDVI, a low cutoff NDVI value was also evaluated. However, applying a lower boundary to the NDVI values reduces pixels on all images, unlike the three image criterion which only reduces pixels on the few affected images. Using a lower boundary is also less apt at removing all the erroneous pixels (Fig. 3c). By using a lower boundary, it is impossible to remove erroneous pixels without affecting non-erroneous pixels on all images, which becomes especially problematic when higher values are necessary to remove all erroneous pixels. Given the good results of the "three image criterion" for the MCB data set, this method was applied to all study areas.

2.4.4 Mudflat extent during low tide exposure and tidal height

The effect of tidal height on the visible extent of the mudflat during low tide exposure was checked for MSM. The visible extent was determined using the number of pixels of the mudflat visible on each image ("pixel count"). Since the sinusoidal projection represents areas accurately, the pixel count gives a good idea of the extent of the exposed mudflat, an approximation in km^2 is given in Table 1. Tidal height was calculated for station St. Malo, using the online tide calculator on the website of the French Service Hydrographique et Océanographique de la Marine (http://www.shom.fr/). The capture time for each image was derived from the images on the OceanColor website. The time obtained in this way does not necessarily correspond to the true capture time of the mudflat pixels, as the L2G

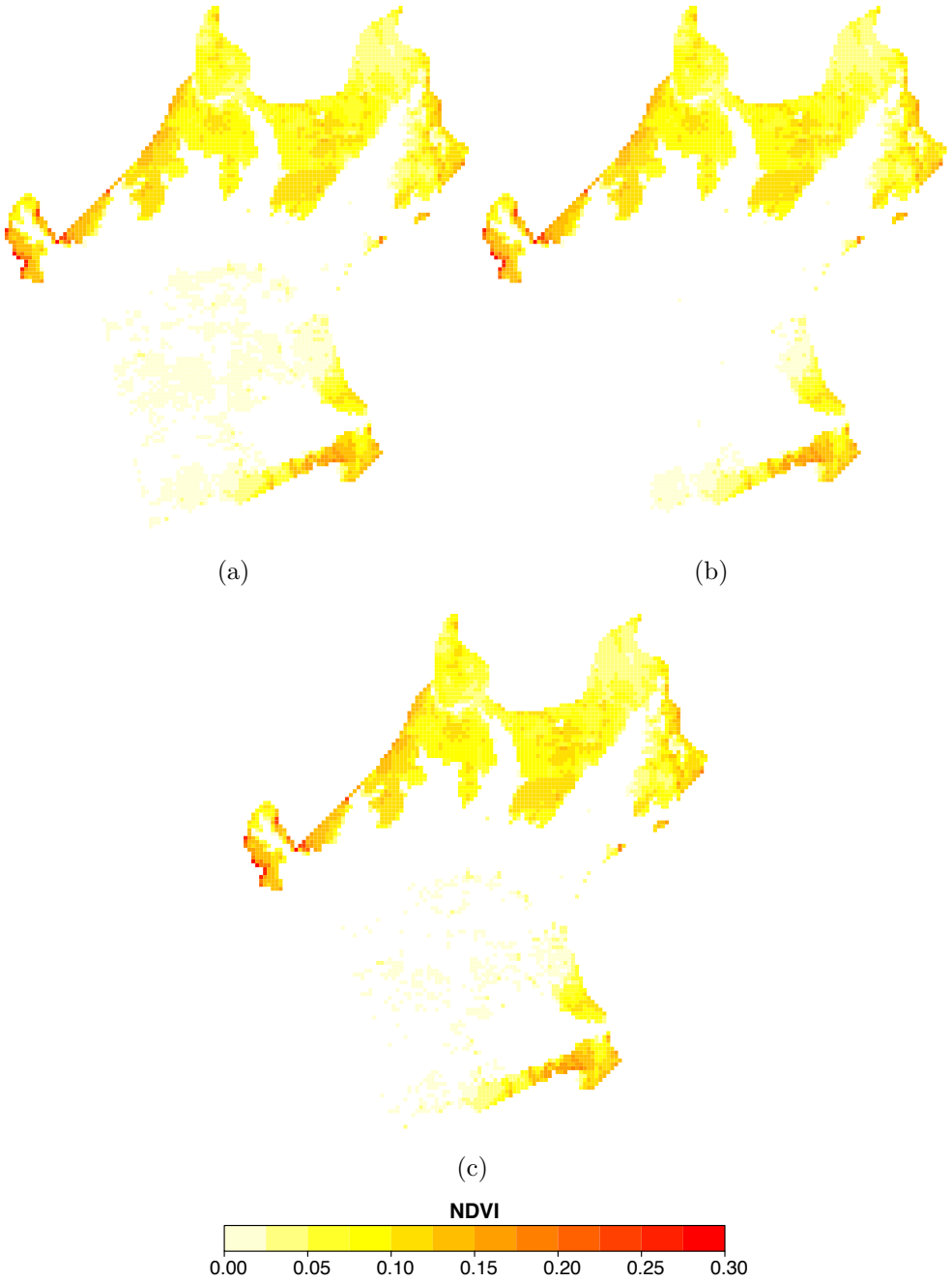

Figure 3: The mapped NDVI of the MCB image taken on 9 April 2003, (a) before and (b) after the removal of pixels that occurred on less than three images in 2003. Note the reduction of the erroneous pixels in the centre and lower left portions of the image, and how the mudflat area is unaffected. The application of a lower limit of 0.015 to the NDVI values did not yield good results (c).

images are a composite of adjacent overpasses. Still, given the match between the mudflat extent on the L2G images and the L0 images, we can be quite confident of the time obtained this way. As the used tidal heights are not observations, but calculations, the actual tidal height at the moment of capture can vary, for example, as a result of wind action. However, the relation between pixel count and tidal height is clearly linear (Fig. 4a), and highly significant ($p < 0.0001$).

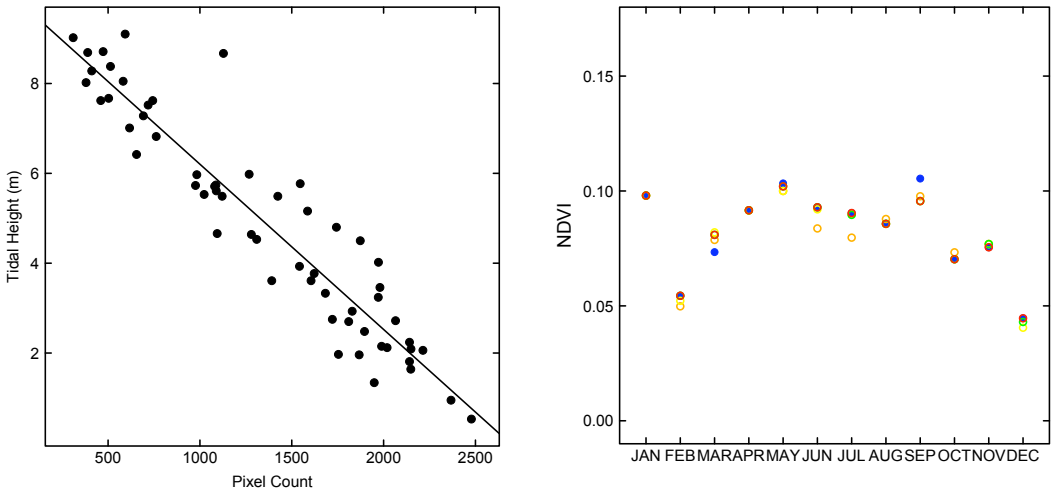

(a) (b)

Figure 4: (a) The linear relation for Mont Saint–Michel Bay between tidal height in reference to Lowest Astronomical Tide, and pixel count (R^2= 0.89, p<0.0001). Tidal height was calculated using the tide calculator of the French Service Hydrographique et Océanographique de la Marine (SHOM) for station St. Malo. The approximate capture time of each image was obtained from OceanColor. (b) The effects of using different pixel count cutoff values on the monthly mean NDVI of the Western Scheldt estuary. The solid blue dots correspond with the monthly mean calculated using all images. The open circles correspond with a certain cutoff value: red for 5 %, green for 10 %, yellow for 20 % and orange for 50 %.

Images with a very low pixel count – captured during or near high tide – tend to have a much higher NDVI and a higher variability than other images. This is probably caused by the fact that a low number of observations does not represent the entire mudflat (in statistics: "the law of small numbers"). Causes of a higher NDVI can be (1) the inclusion of some high elevation, non-mudflat pixels (e.g. salt-marsh vegetation), the effect of which only becomes apparent on images with low pixel counts, or (2) the bias towards zones with higher elevation that generally have a higher production (see also section 3.5). Because no weighting was applied

when calculating monthly and seasonal means, these images with a higher NDVI can have a significant effect on the means. After the initial processing described above, high-tide and almost-high-tide images still included in the data set were excluded using a lower limit on pixel count. To determine the optimal limit, we tested several percentages of the maximum observed pixel count per area (Fig. 4b). For some months, the difference between the mean calculated using a 5 % cutoff and the mean calculated using all images is rather large. The monthly mean varies little between the use of a 5 %, a 10 % or a 20 % cutoff, which is a good indication of the robustness of the data. With a drastic 50 % cutoff some changes are observed, but in general, the pattern remains remarkably unaltered. Thus, when using a lower limit on pixel count, the monthly means yields more representative NDVI values for the mudflat. The 5 % cutoff was applied for all areas, with similar results. Although the images with only 5 % can contain some mudflat pixels with a high microphytobenthos biomass, these images were still excluded because the effect of non-mudflat pixels (e.g. salt-marshes) is too large on the image mean of images with a low pixel count. This can cause erroneous pixels to have a disproportionally large effect on the monthly means. For images with a greater pixel count, these erroneous values do not have such a large effect on the observed means, due to the large number of true mudflat pixels.

2.5 Data analysis

After completion of the quality control and data processing, out data set consisted of NDVI values for each mudflat pixel on each image.

For each image, we calculated the mean and standard deviation of the NDVI. Subsequently, these were used to calculate the mean and standard deviation for each area. A boxplot was created that contains the median, first and third quartiles, the non-outlier minimum and maximum and the outliers per area. Images were grouped per month, and the mean for each month was calculated per area. Monthly means calculated with less than two images were excluded, and the remaining data was plotted. Based on their latitudinal position (rounded off to the nearest full degree, see positions in Table 1), the study areas were grouped in three broad climate zones (see Table 4 for detailed climate information); (1) A tropical climate class (latitudes 0°–20°): FRG, PAP and MOZ. These climates have a high temperature throughout the year, with a very small temperature range. They are characterized by a wet and dry season. (2) A Mediterranean and subtropic climate class (latitudes 20°–40°): SFR, GOM and ARI. These areas have a mild winter and a hot summer, with a rather large temperature range. They have either a wet or a dry summer. (3) A temperate climate class (latitudes > 40°): FOT, MCB, WES, MSM, FCB and SSE. These areas have a mild winter and a mild summer,

with a rather large annual temperature range. They generally have a uniform precipitation distribution throughout the year. Per area, image means were grouped per season: winter (Dec-Feb), spring (Mar-May), summer (Jun-Aug) and autumn (Sep-Nov). These categories are based on the seasons on the northern hemisphere, thus for the sites on the southern hemisphere, the seasons are actually named in reverse. For each season, the mean NDVI value was calculated and NDVI maps were constructed with the seasonal averages of each pixel. The mean NDVI was calculated per area for each season.

Next, we examined if the pattern obtained by using the mean image NDVI could be considered equal over the entire mudflat. In order to determine elevation zones, we calculated for each pixel the number of images it was present on in our data set. As pixels on higher elevation zones are present on both high and low tide images, these occurrences are a good representation of elevation (see also 3.5). The occurrence counts were converted to percentages and five subsets were created: 0–20, 20–40, 40–60, 60–80, and 80–100 %. For each of these zones we calculated the mean NDVI per image. The patterns of these different elevation zones were analyzed in more detail for WES and MSM. In addition to differences caused by elevation, the time since exposure is likely to influence the NDVI values, since it takes a while for microphytobenthos to migrate to the surface. Images captured some time after exposure are expected to have a larger NDVI. A reduction is expected on mudflats that have been exposed to high light conditions for several hours, as a result of downward migration caused by light inhibition. This hypothesis was tested for MSM by plotting NDVI in function of time since exposure, i.e. the time between image capture and the nearest low tide.

3 Results

3.1 Annual variation

To assess the within and between site variations in mean, maximum and minimum observed NDVI per mudflat, a boxplot was created using the mean NDVI of all images per site (Fig. 5). This graph immediately reveals a very large within-area range of the NDVI. The differences between the sites also seem to be quite substantial. The main trend is a gradual increase in biomass from the equator to sites at higher latitudes. The highest mean biomass is observed in the two study sites in the highest latitudes (FOT and SSE), while the lowest biomass is observed near the equator (PAP). The within-site variation seems to be linked with the mean NDVI value, and thus follows a similar trend: a high variation near the poles, and a lower variation near the equator. Three stations seem to deviate from this general trend: SFR, ARI and FCB, sites with a Mediterranean, subtropic and cold temperate climate respectively.

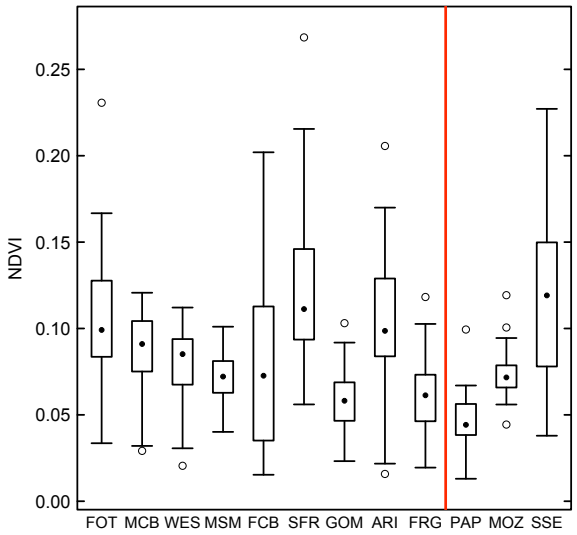

	Mean	σ
FOT	0.106	0.042
MCB	0.088	0.022
WES	0.080	0.022
MSM	0.071	0.015
FCB	0.075	0.045
SFR	0.127	0.051
GOM	0.060	0.017
ARI	0.101	0.045
FRG	0.061	0.021
PAP	0.048	0.020
MOZ	0.074	0.012
SSE	0.119	0.046

Figure 5: Boxplots for the mean NDVI of all included images per area. Plotted are the median (solid dot), first and third quartile (bottom and top of the central rectangle), the non-outlier minimum and maximum (lower and upper whiskers) and outliers (open dots). Note that the whiskers do not represent the standard deviation. Areas are sorted north to south from left to right. The red line is plotted to easily distinguish between the northern and southern hemispheres. The mean and standard deviation are given in the table.

3.2 Annual trend

The mean NDVI for each month was calculated per area. Figure 6 shows the year-round variation of the NDVI per study area. Most temperate sites (green) show a low NDVI value during winter, a sharp increase in NDVI during spring and summer, with a decline starting in autumn. Since SSE is situated in the southern hemisphere, the observed maximum NDVI surprisingly occurs during the austral winter, and the minimum during the austral summer. The Mediterranean and subtropical sites (yellow) have a very large variation during the course of the year, but also between sites. A late winter and early autumn peak, and a clear spring and summer minimum are found for SFR. For GOM we find a pattern with less variation, with peak values towards late winter and early summer. Low NDVI values are observed for spring and autumn. Due to the high number of missing values for ARI, the observed pattern, with the highest NDVI values in late spring, and the lowest in winter, is not complete. We find little variation in monthly mean NDVI values for the study areas in the tropics (blue), which at first glance corresponds to the absence of seasonality in temperature in the tropics. The low NDVI for PAP during June was calculated using only two images with a very low mean NDVI.

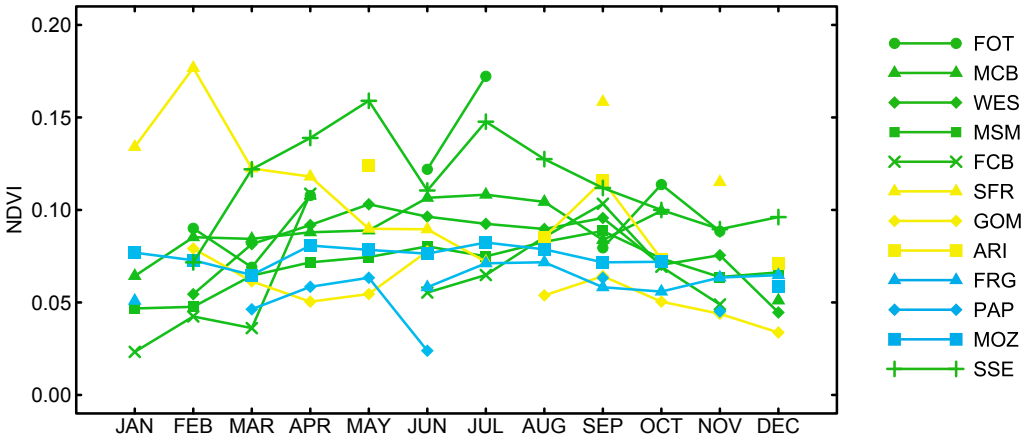

Figure 6: The observed monthly mean NDVI per study area. The colours represent the following latitude ranges: green for latitudes $> 40°$, yellow for latitudes $20°$–$40°$, and blue for latitudes $0°$–$20°$.

3.3 Seasonal trends

For most areas, we find the highest seasonal NDVI values during spring or summer (Table 2). In autumn, a decreased NDVI is observed, which is still higher than the values in winter. Note that for SSE (on the southern hemisphere) the NDVI maximum actually occurs during autumn and winter. For MSM, the highest NDVI is observed in autumn, but is not that different from the spring and summer values. Surprisingly, the highest NDVI value for SFR occurs during winter. Two extremely low seasonal mean values are observed for FRG in spring and PAP in summer, but the number of images used to calculate these values is low (n=2). Based on Fig. 5, it seems that the standard deviation of FCB is much higher than areas such as WES and MSM. For most seasons however, this is not the case, which suggests that most of the variation in FCB occurs between the seasons. For ARI and SFR, a high standard deviation occurs throughout the year. A rather high standard deviation is also observed for SSE during spring and winter.

Table 2: The seasonal mean NDVI per study area. The highest mean per area is underlined. The number of images used to calculate means for each season are given in column "n". Note that for sites on the southern hemisphere (under the dashed line) the season names are reversed.

	Winter (Dec–Feb)			**Spring** (Mar–May)			**Summer** (Jun–Aug)			**Autumn** (Sep–Nov)		
	Mean	σ	n	Mean	σ	n	Mean	σ	n	Mean	σ	n
FOT	0.0857	0.0762	5	0.0844	0.0473	7	<u>0.1261</u>	0.0657	6	0.0743	0.0459	10
MCB	0.0623	0.0304	12	0.0839	0.0312	22	<u>0.0966</u>	0.0392	8	0.0798	0.0411	10
WES	0.0522	0.0241	14	<u>0.0780</u>	0.0376	12	0.0753	0.0403	14	0.0757	0.0346	11
MSM	0.0471	0.0261	10	0.0641	0.0297	20	0.0671	0.0335	18	<u>0.0686</u>	0.0388	10
FCB	0.0600	0.0416	6	<u>0.0938</u>	0.0475	8	0.0767	0.0367	8	0.0875	0.0439	14
SFR	<u>0.1992</u>	0.1115	11	0.1207	0.0504	10	0.0697	0.0372	8	0.1168	0.0731	8
GOM	0.0639	0.0329	7	0.0491	0.0231	14	<u>0.0702</u>	0.0339	6	0.0457	0.0195	15
ARI	0.0737	0.0620	7	0.1000	0.0646	6	<u>0.1005</u>	0.0518	3	0.0805	0.0484	11
FRG	0.0537	0.0298	11	0.0213	0.0193	2	<u>0.0572</u>	0.0356	18	0.0426	0.0293	32
PAP	0.0425	0.0261	2	<u>0.0514</u>	0.0259	6	0.0247	0.0268	2	0.0432	0.0306	6
MOZ	0.0603	0.0316	9	<u>0.0607</u>	0.0350	10	0.0591	0.0377	12	0.0567	0.0303	15
SSE	0.0724	0.0337	6	<u>0.1084</u>	0.0809	18	0.0938	0.0780	14	0.0733	0.0513	20

3.4 Seasonal patterns in spatial distribution within mudflats

Seasonal maps were created for all study areas, but only those of WES and MSM were examined in detail, since more literature is available on microphytobenthos dynamics in these areas. The seasonal maps for WES and MSM are shown in Fig. 7.

3.4.1 Western Scheldt estuary

For WES (Fig. 7a-d), a clear winter low and a sharp increase between winter and spring mean NDVI values are observed (Table 2). The spring increase in NDVI occurs on several mudflats of WES (Fig. 7b). On some mudflats this high NDVI persists throughout the summer while on others, the NDVI decreases again. The increase in NDVI values during summer occurs on different mudflats (Fig. 7c). The high NDVI on the mudflats in summer persists during autumn. The highest NDVI values can be observed towards the centre of the flats, which have the highest elevation. The mean NDVI value decreases somewhat after spring, but does not reach the low value observed in winter. Standard deviation is lowest in winter, and highest in summer, but not much different from spring and autumn values.

3.4.2 Mont Saint-Michel bay

For MSM, we observe a low NDVI during winter with a clear increase towards spring. The highest NDVI occurs during autumn, but does not deviate much from NDVI values found in spring and summer (Table 2). Both of these trends are very similar to the ones found for WES. The spatial structure of the NDVI reveals that most of the high NDVI values occur in the westernmost region of the bay, as well as some fringing areas in the eastern part (Fig. 7e-h). The NDVI values in the westernmost part are more spread out and lower in spring than in summer. In autumn, the observed higher NDVI values are more extensive than in summer, but they have the same magnitude. The zone in which the highest biomass occurs seems to move and change in size over the course of the seasons. A few fringing pixels in the eastern part have a high NDVI during the entire year. In summer and autumn, the NDVI values in the eastern part increase, and a more extensive area with higher NDVI develops around them. The standard deviation increased with increasing seasonal means, from winter to autumn. The standard deviations for MSM are among the lowest we observed.

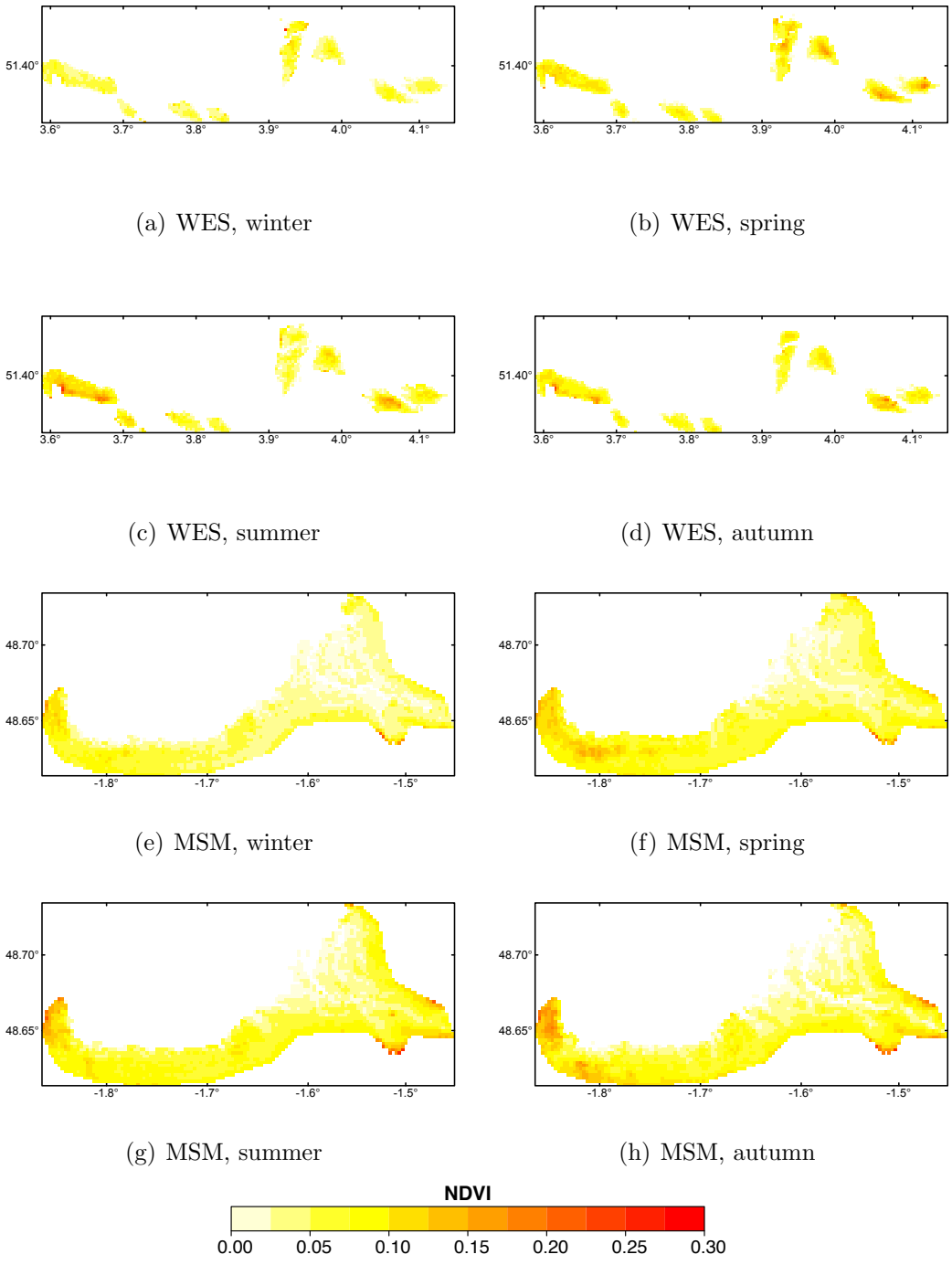

(a) WES, winter

(b) WES, spring

(c) WES, summer

(d) WES, autumn

(e) MSM, winter

(f) MSM, spring

(g) MSM, summer

(h) MSM, autumn

Figure 7: The mapped NDVI of the Western Scheldt estuary (WES) and the Mont Saint-Michel Bay (MSM) for each of the four seasons (Winter: Dec–Feb; Spring: Mar–May; Summer: Jun–Aug; Autumn: Sep–Nov). Latitude and longitude on the vertical and horizontal axis respectively. Note the different scales of the maps of WES and MSM.

3.5 Effects of elevation

To determine whether the observed annual trend based on the mean NDVI values per image can be considered equal over the entire mudflat, the data per area was divided in five elevation subsets. As a pixel with a higher occurrence is present on more images, these zones are very dependent on the available image set for each area. For example, when the data set contains more low-tide images, the upper zone (80–100 %) will on average contain more pixels. Thus, the elevation zones we created are strongly linked to the available images for 2003. However, the subsets based on occurrences seem to correspond with elevation zones in the mudflat (Fig. 8a-b). The correspondence of pixel occurrence with elevation can be seen more clearly on the large intertidal areas, such as MSM. For each image, zones with pixel counts less than 20 were excluded, in order to remove a possible bias on the zone mean. A good correspondence of the annual NDVI patterns of the different zones is observed, as well as a clear positive relation between NDVI and elevation. The results for WES and MSM are given in Fig. 8c-d. The correlation between these patterns is rather high, and in most cases significant (Table 3). Note that the correlations with less or no significance are only found for MSM, when comparing the highest zone (80–100 %) with the zones 0–20 % ($p = 0.0289$) and 20–40 % ($p = 0.2534$), and when comparing the zones 20–40 % and 60–80 % ($p = 0.0132$). This indicates that the patterns in the high and low zones differ somewhat from the rest of the mudflat. The correlation between monthly averaged NDVI patterns is higher, which confirms the reliability of the patterns in monthly NDVI values we observed (Fig. 6).

3.6 Mudflat exposure time

Generally, a delay is observed between the ebbing of the tide and the upward migration of microphytobenthos, as well as between the downward migration after exposure to high light conditions for several hours. We tested if by using coarse resolution MODIS data these changes in microphytobenthos biomass could be observed for MSM. The time between the capture of each image and the moment of low tide was determined using tidal calculations from SHOM. While the relationship appears to be linear (Fig. 9), we could not find a significant trend ($R^2 = 0.07$, $p = 0.049$). A linear regression of the exposure times and NDVI for the different seasons cannot explain the variation in the NDVI (Winter: $R^2 = 0.32$, $p = 0.085$; Spring: $R^2 = 0.16$, $p = 0.077$; Summer: $R^2 = 0.22$, $p = 0.049$; Autumn: $R^2 = 0.64$, $p = 0.006$). In contrast with our hypothesis, the trend for autumn is negative (brown dots in Fig. 9), caused by the absence of images taken long time after exposure. No significant relationship is found between mudflat exposure time and the NDVI of the different elevation zones.

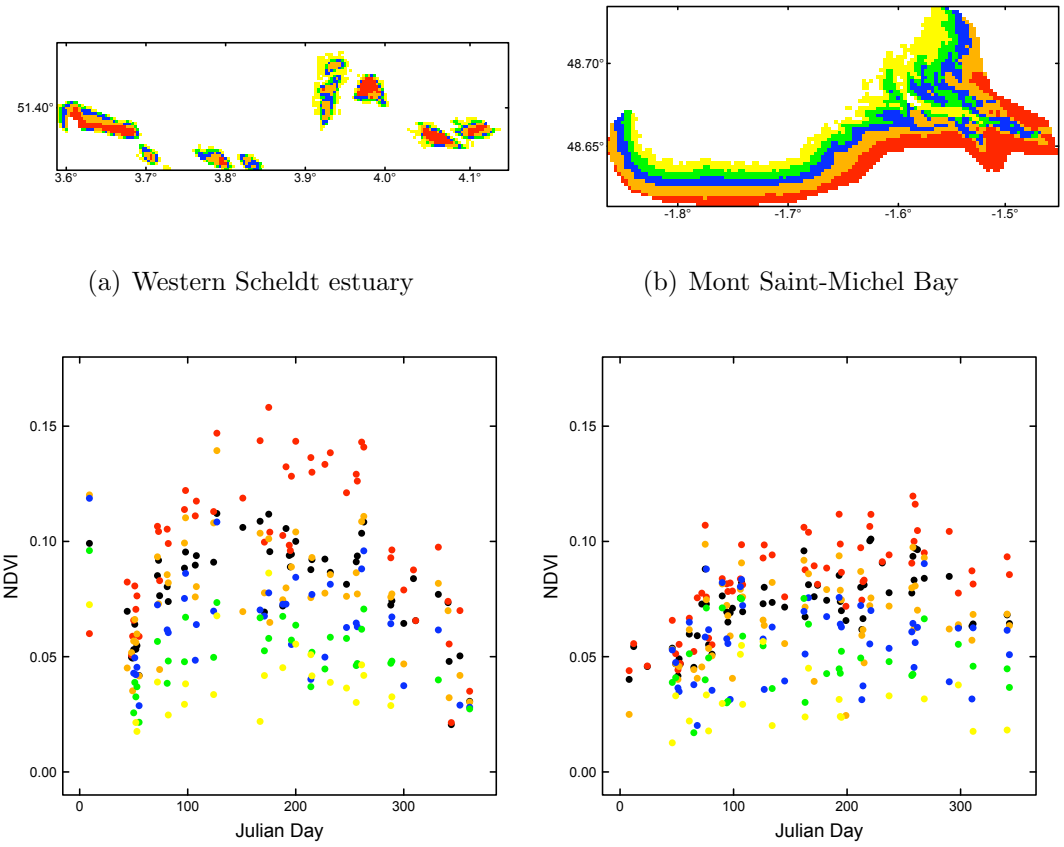

(a) Western Scheldt estuary

(b) Mont Saint-Michel Bay

(c) Western Scheldt estuary

(d) Mont Saint-Michel Bay

Figure 8: The pixel occurrence percentage ranges mapped for (a) the Western Scheldt estuary and (b) the Mont Saint-Michel Bay: 0–20 % (yellow), 20–40 % (green), 40–60 % (blue), 60–80 % (orange), and 80–100 % (red). Latitude and longitude on the vertical and horizontal axis respectively. Note the different scales of the maps. The mean NDVI per image, with the same pixel occurrence percentage ranges, for (c) the Western Scheldt estuary and (d) the Mont Saint-Michel Bay. The solid black dots represent the image mean for all pixels. For an overview of the correlation of the patterns for these zones, see Table 3

Table 3: Spearman's rank correlation coefficients for the NDVI patterns of the different elevation zones from Fig. 8, for (a) the Western Scheldt estuary and (b) the Mont Saint-Michel Bay. Pairwise complete observations were used in order not to exclude images taken during higher tide levels. All coefficients are highly significant ($p < 0.01$), except those in *italic*. The single image from January for the Western Scheldt was omitted from this analysis because it was the only image with a considerably lower mean NDVI for the highest zone.

(a) Western Scheldt estuary

	100 %	**100–80 %**	**80–60 %**	**60–40 %**	**40–20 %**	**20–0%**
100 %	1.000	0.842	0.780	0.746	0.726	0.550
100–80 %	0.842	1.000	0.747	0.606	0.572	0.472
80–60 %	0.780	0.747	1.000	0.868	0.788	0.488
60–40 %	0.746	0.606	0868	1.000	0.890	0.649
40–20 %	0.726	0.572	0.788	0.890	1.000	0.627
20–0 %	0.550	0.472	0.488	0.649	0.627	1.000

(b) Mont Saint-Michel Bay

	100 %	**100–80 %**	**80–60 %**	**60–40 %**	**40–20 %**	**20–0%**
100 %	1.000	0.904	0.686	0.502	0.387	0.504
100–80 %	0.904	1.000	0.737	0.388	*0.152*	*0.287*
80–60 %	0.686	0.737	1.000	0.796	*0.324*	0.344
60–40 %	0.502	0.388	0.796	1.000	0.766	0.340
40–20 %	0.387	*0.152*	*0.324*	0.766	1.000	0.614
20–0 %	0.504	*0.287*	0.344	0.340	0.614	1.000

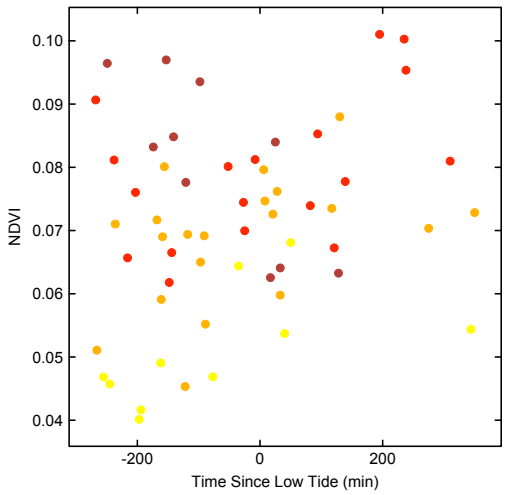

Figure 9: The relationship between time since low tide (with negative values referring to the time before low tide) and mean image NDVI for the Mont Saint-Michel Bay. Yellow, orange, red and brown dots represent winter, spring, summer and autumn respectively. An increasing trend can be discerned, which is, however, not significant ($R^2 = 0.07$, $p = 0.049$).

4 Discussion

This study was performed in order to (1) explore the suitability of MODIS remote sensing data to study large-scale temporal and spatial trends in intertidal microphytobenthos biomass, and (2) use MODIS remote sensing data to assess such trends in twelve extensive intertidal areas worldwide.

4.1 Evaluation of MODIS data

While we experienced some problems related to the nature of the L2G images on the one hand, and to our automated processing on the other hand, MODIS imagery appears to be very suitable for the study of microphythobenthos on intertidal areas (see further). However, as not only microphytobenthos biomass can affect the NDVI values on the mudflats, some additional considerations have to be made when using MODIS L2G data. (1) Using the NDVI it is impossible to differentiate between microphytobenthos and other vegetation, thus knowledge of the vegetation distribution for each area is indispensable. (2) Considerable changes in the exposed area of the mudflat are caused by the timing of the tidal cycle and the daily MODIS overpass, which falls within a window of about 2.5 hours. Thus, since there is a positive relationship between NDVI and elevation (see 3.5), the observed NDVI values can differ substantially from the actual NDVI values. Additionally, an increase of the solar zenith angle increases NDVI values (Jackson and Huete, 1991), as the height of the sun has a larger effect on the reflectance in the red band than on the reflectance in the near-infrared band. A rigorous calibration of the image set, based on the lightest and darkest invariable pixel per area, can possibly reduce this effect, but was not within the scope of this research. (3) The length of mudflat exposure at the time of capture also affects the NDVI values, mainly caused by the migration of the microphytobenthos. Colonization of the mudflat by microphytobenthos after emersion is reported to occur within 15 minutes (Herlory et al., 2004). Additionally, a downward migration of the microphytobenthos occurs at the rising of the tide and as a result of high light intensities and desiccation (Perkins et al., 2001). Furthermore, since the NDVI is directly related to soil water content (Jackson and Huete, 1991), dessication will also cause NDVI values to drop after a long tidal exposure. However, a clear relationship between NDVI and time since exposure could not be found using MODIS data (Fig. 9). Thus, the migratory behaviour of the microphytobenthos will probably not have a substantial effect on the NDVI ranges observed on intertidal flats with a coarse resolution sensor.

4.2 Annual variation and seasonal trends

When comparing the mean and the annual ranges of the NDVI (Fig. 5), sites near the equator seem to have a smaller NDVI, coupled with a smaller variation during the year. For sites with increasing latitudes, we find an increasing NDVI, coupled with an increasing variation throughout the year. Three sites seem to deviate from this general pattern: FCB, SFR and ARI. Spearman's rank correlation between mean NDVI and latitude (rounded off to nearest full degree) is 0.601 ($p = 0.039$) with all sites included, and 0.833 ($p = 0.005$) without FCB, SFR and ARI. This indicates an increase in average annual microphytobenthos biomass (per pixel) towards the poles, within the latitude range of the studied areas. For most areas, the highest seasonal NDVI values are observed during spring or summer. A slightly lower NDVI is observed in autumn, which is still higher than winter NDVI. For SFR and MSM, the highest seasonal mean occurs during winter and autumn respectively. The correlation between standard deviation and annual temperature ranges are not significant however. For most sites, the standard deviation varies little over the seasons, which indicates that the seasonal values we find are quite robust. For the two smallest sites in our study, FOT and SFR, we observe a large mean NDVI and a large standard deviation. The effects of erroneous pixels, such as non-mudflat or mixed pixels, probably become too large with a smaller pixel count. In comparison with their pixel count, the smaller areas have a larger boundary to the terrestrial environment, which increases the occurrence of mixed pixels. As the tidal range is very variable for SFR, the number of images with a pixel count larger than 100 is limited to ten out of the thirty-three images included in the study.

The highest NDVI for MSM is observed in autumn, but is not that different from the spring and summer values. Similarly, the seasonal NDVI values for WES do not differ much between spring, summer and autumn. For SSE, the maximum NDVI actually occurs during autumn and winter since it is located on the southern hemisphere. The SSE pattern deviates somewhat from the expectation of a low NDVI during the months June–August. Instead we observe a high NDVI during these months, and a low NDVI during November, December and February (no images for January). For all of our temperate sites, with a uniform precipitation distribution (Table 4), we find significant correlations between NDVI and temperature, see Table 5. The correlation is positive for all sites except SSE, which is also reflected in the pattern in Fig. 6. Note that the correlation with temperature can also represent a correlation with a related factor such as insolation. For a mudflat in WES, Sabbe (1993) found a better correlation between the spring bloom of epipelon and insolation than between the spring bloom and temperature.

Surprisingly, the highest NDVI value for SFR occurs during winter, with the lowest values occurring during summer (Table 2). Images for ARI are spread out and rather grouped over the year, so a good annual pattern cannot be obtained. However, we find a maximum NDVI in spring and summer, and a minimum during winter. For both ARI and SFR, a high standard deviation occurs throughout the year. There is a significant positive correlation between the monthly NDVI and the precipitation for SFR and ARI (Table 5), with high NDVI values occurring during wetter conditions. For SFR, an almost significant ($p = 0.055$) negative correlation between temperature and NDVI is observed. The hot and dry conditions during summer seem to have a large effect on the microphytobenthos biomass in SFR, while the microphytobenthos in ARI seems to be only affected by precipitation. In contrast with our results for ARI, a winter high in biomass was observed by Koh et al. (2007), who suggested that the winter conditions favoured the microphytobenthic assemblage of these flats.

The patterns obtained for FRG, PAP and MOZ, the sites with a tropical climate seem to correspond with the absence of seasonality in temperature (Table 4). An effect of the drier season, which typically occurs between May and October, is not observed. No significant correlations between NDVI and temperature or precipitation are found (Table 5). Two very low means are observed for FRG in spring and PAP in summer, but this is likely to be an artefact caused by the low number of images (n=2) used to calculate these means. As the mean NDVI per image is much lower than the values throughout the year, these values probably do not represent the seasonal mean very well. Some remaining low NDVI values not caused by mudflat pixels, e.g. NDVI values in adjacent waters, can also be observed on these images. Other possible causes for these anomalous values are increased grazing on the microphytobenthos or a drastic reduction of their biomass by large storms.

4.2.1 Seasonal patterns

For WES, we find a clear winter to spring increase in NDVI, with lower values in summer and autumn than in spring (Table 2). The spring increase in NDVI is present on several mudflats of WES (Fig. 7b). On some mudflats this high NDVI persists throughout summer, while on others the NDVI decreases. On yet other mudflats, a first increase of NDVI occurs during summer (Fig. 7c). The mudflats from WES with a high NDVI occurring during summer that persists throughout autumn are probably also populated by macroalgae or higher plants (Sabbe, *pers. comm.*). On the Molenplaat, the northernmost mudflat on Fig. 7a-d, the microphytobenthos biomass increases sharply during May and June, and decreases again towards the end of summer (Stapel and de Jong, 1998).

Table 4: Climate data per study area. Temperature (T) in degrees Celcius, and precipitation (P) in mm. Note that these are multiple-year climate data, and do not directly represent the weather of 2003. Data was obtained from the closest available station. No precipitation data for GOM could be obtained.

	FOT [1]		**MCB** [1]		**WES** [2]		**MSM** [3]		**FCB** [3]		**SFR** [3]	
	T	P	T	P	T	P	T	P	T	P	T	P
Jan.	3.2	68.6	4.3	81.1	3.2	61.8	5.3	92.8	-8.4	86.6	8.6	77.2
Feb.	3.5	45.8	4.4	58.7	3.3	44.3	4.9	69.9	-7.7	72.8	10.7	63.5
Mar.	4.5	49.5	6.1	68.3	5.3	56.9	6.3	62.8	-2.9	78.6	12.0	59.9
Apr.	5.5	43.9	7.9	48.9	8.0	46.4	7.5	53.2	3.0	74.1	13.6	27.4
May	6.8	49.5	11.1	49.0	12.0	48.8	10.7	49.3	9.7	74.7	15.8	4.8
June	8.4	51.1	13.7	59.8	14.9	61.8	13.3	43.4	14.8	84.4	18.1	1.7
July	9.5	46.8	15.9	59.5	16.9	68.0	15.5	51.9	18.5	88.9	19.1	1.0
Aug.	9.5	47.2	15.9	73.4	17.3	68.0	15.7	63.1	17.6	81.8	19.1	1.5
Sept.	8.1	61.7	13.6	82.5	15.3	62.0	14.2	74.2	13.1	78.6	18.3	5.0
Oct.	6.4	66.4	10.5	97.9	12.0	79.6	11.7	108.9	7.6	90.6	15.7	21.5
Nov.	4.5	57.3	7.1	94.0	7.4	75.0	8.2	117.4	1.8	91.6	11.8	53.0
Dec.	3.5	66.2	5.1	98.3	4.6	72.7	6.3	111.8	-5.5	86.9	8.7	62.9

	GOM [3]		**ARI** [3]		**FRG** [3]		**PAP** [4]		**MOZ** [3]		**SSE** [3]	
	T	P	T	P	T	P	T	P	T	P	T	P
Jan.	-0.3	–	6.3	74.9	25.4	385.4	26.7	229.9	27.4	267.0	10.6	27.4
Feb.	0.8	–	6.7	87.2	25.6	330.2	26.7	261.4	27.4	258.6	10.0	32.0
Mar.	5.1	–	9.9	123.5	25.8	397.4	26.8	278.5	26.7	262.9	8.1	27.7
Apr.	11.5	–	14.7	190.3	26.0	430.9	26.8	160.1	25.3	116.8	6.0	34.0
May	16.8	–	18.5	190.5	25.8	545.9	26.2	90.5	22.8	66.5	2.6	37.8
June	21.3	–	22.0	326.3	25.5	398.6	25.2	35.2	20.8	39.9	0.3	26.0
July	25.1	–	26.2	283.9	25.6	202.7	25.0	23.1	20.4	33.8	0.1	27.2
Aug.	25.9	–	27.2	186.9	26.1	108.0	25.0	25.4	21.2	33.0	2.3	11.7
Sept.	21.4	–	24.0	236.4	26.5	42.3	25.5	41.6	23.0	25.1	3.5	19.3
Oct.	15.3	–	18.7	107.8	26.7	49.7	26.5	45.9	24.8	34.2	6.1	29.1
Nov.	8.5	–	13.4	88.7	26.2	126.5	26.9	68.9	26.1	121.0	8.1	34.1
Dec.	2.6	–	8.6	79.9	25.7	298.5	27.1	148.2	26.9	243.3	9.5	32.5

Climate data obtained from:
(1) http://www.metoffice.gov.uk/, (2) http://www.climate-charts.com/,
(3) http://www.worldclimate.com/, (4) http://commons.wikimedia.org/.

Table 5: Spearman's rank correlation between the monthly NDVI and the temperature and precipitation data per site. Significant ($p < 0.05$) correlations in **bold**. No precipitation data could be obtained for GOM.

Code	Temperature		Precipitation	
	r_s	p	r_s	p
FOT	**0.647**	0.023	-0.143	0.658
MCB	**0.791**	0.002	-0.418	0.176
WES	**0.656**	0.021	-0.328	0.298
MSM	**0.907**	0.001	-0.448	0.145
FCB	**0.648**	0.023	-0.158	0.624
SFR	-0.567	0.055	**0.783**	0.003
GOM	0.164	0.611	–	–
ARI	0.300	0.343	**0.900**	0.001
FRG	0.095	0.768	-0.190	0.553
PAP	-0.058	0.858	0.314	0.320
MOZ	-0.492	0.104	-0.255	0.425
SSE	**-0.715**	0.009	-0.082	0.800

We observe a consistently higher NDVI throughout the year in the western part of MSM (Fig. 7e–h). Davoult et al. (2009) observed a high biomass in the westernmost part of MSM, and a lower biomass on a more eastern transect. The higher primary production in the western part, which is more sheltered than the rest of the bay (Davoult et al., 2009), is probably caused by the muddy substrates in that area. Although some cultivation of mollusks takes place in the western areas, Riera (2007) has shown that microphytobenthos does not contribute significantly to their diet. The group of pixels in the east, with a high NDVI throughout the entire year probably are some salt-marsh pixels included in the ROI, see map in Riera (2007). We find an increasing NDVI from winter to autumn (Table 2), but with shifting zones of high biomass, (Fig. 7 e-h). In another site in the eastern English Channel (Somme Bay), Migné et al. (2004) observed a clear seasonal pattern in microphytobenthos biomass, with a summer maximum. Davoult et al. (2009) on the other hand, could not observe a seasonal trend, and in addition, they found a summer minimum in biomass. On two sites near MSM, Migné et al. (2004) and Spilmont et al. (2006) observed a low in microphytobenthos production in January–February, and a high in June–July. However, a high biomass does not necessarily represent a high primary production (Davoult et al., 2009). These results show that the biomass of microphytobenthos in the English Channel is very dynamic and can vary as a result of many factors. Also note that our data set contains more observations (58 images) than the ten or twelve observations, or even only one observation per season when working with transects, in other studies.

Although the seasonal microphytobenthos dynamics are less well known or not described for most study areas, we expect that our results for the other areas are of similar quality as these for WES and MSM.

4.2.2 Elevation effects

When considering the different elevation zones in Fig. 8 the mean pattern is a good representation of the mudflat seasonality. The patterns of the higher zones have a high correlation with the mean pattern, while the correlation with the lower zones is less strong. The higher correlation between adjacent areas also indicates greater similarity between them. We observe a higher biomass on the higher levels of the mudflat, and a lower biomass on the lower levels. These results are in good agreement with previous research (Admiraal and Peletier, 1980; Colijn and de Jonge, 1984; Thornton et al., 2002). For WES, we observe a higher NDVI increase during summer in the highest zone (pixels present on 80–100 % of the images), which is probably caused by the presence of vegetation other than microphytobenthos on some parts of the mudflats (Sabbe, *pers. comm.*). If pixels with vegetation other than microphytobenthos are included for MSM, their effects are less clear, possibly due to the larger size of the mudflats.

4.3 Exposure time

With increasing emersion time, a steady increase in microphytobenthos biomass has been observed using *in situ* sampling and measurements, for example by Blanchard et al. (1998). Using MODIS data, we did not observe a significantly higher production on images that were captured after a longer mudflat exposure time (Fig. 9). Considering the substantial annual and daily variation of microphytobenthos biomass, this is probably caused by the fact that the images with different exposure times were all taken during a different time of the year, and that the tidal cycle changed in respect to the day-night cycle. The error margin on the capture time, and the differences between the calculated tidal height and the actual tidal height can also contribute to the noise in this relation, however, not in a large degree, considering the good results presented in Figure 4a. This seemingly disappointing result is not that important since we used MODIS imagery, with a maximum temporal resolution of one day, to assess a pattern that exists on much smaller temporal scales, i.e. during a single emersion.

5 Conclusions

5.1 Evaluation and processing of MODIS data

MODIS L2G images have their weaknesses and pitfalls related to the automatic generation and atmospheric correction. Nonetheless, for large-scale research – with a couple of hundred images – they prove to be quite reliable. We used automated processing methods to cope with the large data set. While our results do show some artifacts related to this highly automated processing, our methods deliver promising results, with room for improvements. We find that the NDVI calculated using the MODIS L2G data are robust enough for the analysis of microphytobenthos biomass on intertidal areas. The results for smaller areas and areas with a rather complex structure are not as robust due to the coarse ground resolution and the disproportionate effect of mixed pixels and non-mudflat pixels.

5.2 Trends

MODIS images are very valuable for determining large-scale temporal and spatial patterns of intertidal microphytobenthos biomass. Using these data, it is possible to determine clear seasonal patterns that are significantly correlated with local climate characteristics. An increasing NDVI and an increasing effect of temperature variation – and thus, seasonality – is observed towards the poles. In tropic sites, we find low NDVI values and a low variation throughout the year. No correlations with temperature or precipitation are found, which corresponds to the aseasonal character of the tropics. The microphytobenthos in study areas on latitudes around 30° seem to be mainly affected by the precipitation regime. Within-site variability remains rather large in our data set for 2003. We have shown that the general seasonal trends can be considered equal over the entire intertidal area, albeit with a lower NDVI on the lower, and a higher NDVI on the higher elevation zones of the mudflat. This trend characterizes the microphytobenthos development on intertidal flats in turbid waters. That it can be observed using MODIS images is very reassuring. The spatial and seasonal patterns we observe for WES and MSM are in agreement with results in literature. The patterns for autumn seem to differ somewhat, possibly due to the inclusion of some macroalgae or salt-marsh vegetation, which increases the mean NDVI of some images considerably. Perhaps this higher NDVI can be used to exclude certain pixels from the data, but further study is needed. We also should note that by using MODIS images, the number of observations in one year can be up to five times higher than what is possible with classic *in situ* measuring methods. However, field data are of great value to remote sensing applications. In general, a better knowledge of the study areas, the inclusion of field data, and the acquisition of

data for multiple years will improve our results. Data from multiple years will reduce the effects of large daily fluctuations and thus will provide more correct annual and seasonal patterns.

5.3 Perspectives

The results we obtained could certainly be improved upon. As stated above, the use of images from multiple years will increase the robustness of our results, but other improvements can easily be formulated. The NDVI on high and low elevation zones on the mudflat is not in good correspondence with the mean NDVI of the mudflat. Therefore, it would be feasible to examine the results of using only the central part of the mudflat. For example, by using only the pixels present on 10–90 % or on 20–80 % of the images. Our results have shown that it is very valuable to have knowledge on the occurrence of macrophytes and salt-marsh vegetation. Even for mudflats in developed countries, detailed maps documenting their presence are not easily obtained. Therefore it is desirable to explore methods that can differentiate between macrophytes, salt-marsh vegetation and microphytobenthos. Perhaps a simple method, such as determining the sensor-specific upper NDVI limit of microphytobenthos can suffice. As microphytobenthos biomass development is not equal for sand and clay substrates, sediment maps can be used to explain local differences in the study areas. Field data is necessary to better assess the value of the NDVI maps based on MODIS images. A further improvement is possible by using quality information, such as flags for atmospheric correction and cloud cover, from the associated 500 m and 1000 m resolution images, a method that requires a lot of work (Van der Wal, *pers. comm.*). As intertidal areas are sparsely vegetated, the NDVI values are strongly affected by soil reflectance. Perhaps this influence can be reduced by using the Soil-Adjusted Vegetation Index (SAVI). However, the use of SAVI requires a local calibration (Pettorelli et al., 2005), which was not possible in the scope of this research. Nonetheless, the effect of soil reflectance on the NDVI is present in all our study areas, which can reduce this error to some degree when comparing NDVI values between sites. A calibration of the NDVI will also improve our results, but for intertidal areas this is not as straightforward as the calibration of terrestrial areas. This is due to the absence of – considering the coarse resolution of MODIS – very large areas on the intertidal flats that remain constant throughout the year.

Acknowledgements

I would like to thank Koen Sabbe and Aaike De Wever, for their great support and dedication that make this thesis a reality. I am grateful for comments and insights provided by Daphne van der Wal and Rudi Goossens. A big thanks goes to NASA, which made this study possible by providing MODIS images free of charge. I would like to express my sincere thanks to the open source community that provided a stable, powerful and flexible computing environment. Margot Vanhellemont was an inexhaustible source of help and suggestions, concerning statistics, style and language. From the bottom of my heart, I would like to thank my parents for everything they have ever done for me.

And last, but not in the very least bit least, I would like to thank Lien Devos. She fills my every day with happiness and love. It is to her I wish to dedicate my work.

References

Admiraal, W. (1984). The ecology of estuarine sediment-inhabiting diatoms. *Progress in Phycological Research*, 3:269–322.

Admiraal, W. and Peletier, H. (1980). Influence of seasonal variations of temperature and light on the growth rate of cultures and natural populations of intertidal diatoms. *Marine Ecology Progress Series*, 2:35–43.

Baeyens, W., van Eck, B., Lambert, C., Wollast, R., and Goeyens, L. (1998). General description of the Scheldt estuary. *Hydrobiologia*, 366:1–14.

Bates, C. R., Moore, C. G., Malthus, T., Mair, J. M., and Karpouzli, E. (2004). Broad scale mapping of habitats in the Firth of Tay and Eden Estuary, Scotland. *Scottish Natural Heritage Commissioned Report No. 007. (ROAME No. F01AA401D).*

Blanchard, G. F., Guarini, J.-M., Bacher, C., and Huet, V. (1998). Contrôle de la dynamique a court terme du microphytobenthos intertidal par le cycle exondation-submersion. *Écologie*, 321:501–508.

Blanchard, G. F., Guarini, J.-M., Gros, P., and Richard, P. (1997). Seasonal effect on the relationship between the photosynthetic capacity of intertidal microphytobenthos and temperature. *J. Phycol.*, 33:723–728.

Cadée, G. and Hegeman, J. (1974). Primary production of the benthic microflora living on tidal flats in the Dutch Wadden Sea. *Neth. J. Sea Res.*, 8:260–291.

Cahoon, L. B. (2006). Upscaling primary production estimates: Regional and global scale estimates of microphytobenthos production. *Functioning of microphytobenthos in estuaries.*, pages 99–108.

Colijn, F. and de Jonge, V. N. (1984). Primary production of microphytobenthos in the Ems-Dollard Estuary. *Marine Ecology Progress Series*, 14:185–196.

Combe, J.-P., Launeau, P., Carrère, V., Despan, D., Méléder, V., Barillé, L., and Sotin, C. (2005). Mapping microphytobenthos biomass by non-linear inversion of visible-infrared hyperspectral images. *Remote Sensing of Environment*, 98:371–387.

Davoult, D., Migné, A., Créach, A., Gévaert, F., Hubas, C., Spilmont, N., and Boucher, G. (2009). Spatio-temporal variability of intertidal benthic primary production and respiration in the western part of the Mont Saint-Michel Bay (Western English Channel, France). *Hydrobiologia*, 620:163–172.

de Jong, D. and de Jonge, V. (1995). Dynamics and distribution of microphytobenthic chlorophyll *a* in the Western Scheldt estuary (SW Netherlands). *Hydrobiologia*, 311:21–30.

Decho, A. W. (2000). Microbial biofilms in intertidal systems: an overview. *Continental Shelf Research*, 20:1257–1273.

Deppe, F. (2000). *Intertidal Mudflats Worldwide*. Common Wadden Sea Secretariat.

der Wal, D. V. (2008). Evaluation of the performance of satellite imagery versus airborne imagery for the assessment of biophysical variables (preliminary results). *ALGASED Report*.

Deronde, B., Kempeneers, P., and Forster, R. (2006). Imaging spectroscopy as a tool to study sediment characteristics on a tidal sandbank in the Westerschelde. *Estuarine, Coastal and Shelf Science*, 69:580–590.

Fiot, J. and Gratiot, N. (2006). Structural effects of tidal exposures on mudflats along the French Guiana coast. *Marine Geology*, 228:25–37.

Ford, R. and Honeywill, C. (2002). Grazing on intertidal microphytobenthos by macrofauna: is pheophorbide a a useful marker? *Marine Ecology Progress Series*, 229:33–42.

Forster, R., Créach, V., Sabbe, K., Vyverman, W., and Stal, L. (2006). Biodiversity-ecosystem function relationship in microphytobenthic diatoms of the Westerschelde estuary. *Marine Ecology Progress Series*, 311:191–201.

Guarini, J.-M., Cloern, J. E., Edmunds, J., and Gros, P. (2002). Microphytobenthic potential productivity estimated in three tidal embayments of the San Francisco Bay: A comparative study. *Estuaries*, 25(3):409–417.

Hagerthey, S. E., Defew, E. C., and Paterson, D. M. (2002). Influence of corophium volutator and hydrobia ulvae on intertidal benthic diatom assemblages under different nutrient and temperature regimes. *Marine Ecology Progress Series*, 245:47–59.

Herlory, O., Guarini, J.-M., Richard, P., and Blanchard, G. (2004). Microstructure of microphytobenthic biofilm and its spatio-temporal dynamics in an intertidal mudflat (Aiguillon Bay, France). *Marine Ecology Progress Series*, 282:33–44.

Huete, A., Didan, K., Miura, T., Rodriguez, E., Gao, X., and Ferreira, L. (2002). Overview of the radiometric and biophysical performance of the MODIS vegetation indices. *Remote Sensing of Environment*, 83:195–213.

Jackson, R. D. and Huete, A. R. (1991). Interpreting vegetation indices. *Preventive Veterinary Medicine*, 11:185–200.

King, M. D., Kaufman, Y. J., Menzel, W. P., and Tanré, D. (1992). Remote sensing of cloud, aerosol, and water vapor properties from the Moderate Resolution Imaging Spectrometer (MODIS). *IEEE Transactions on Geoscience and Remote Sensing*, 30(1):2–27.

Koh, C.-H., Khim, J. S., Araki, H., Yamanishi, H., and Koga, K. (2007). Within-day and seasonal patterns of microphytobenthos biomass determined by co-measurement of sediment and water column chlorophylls in the intertidal mud-flat of Nanaura, Saga, Ariake Sea, Japan. *Estuarine, coastal and shelf science*, 72:42–52.

Lillesand, T. M. and Kiefer, R. W. (2000). *Remote Sensing and Image Interpretation*. John Wiley and Sons Inc., 4th edition.

MacIntyre, H. L., Geider, R. J., and Miller, D. C. (1996). Microphytobenthos: The ecological role of the "secret garden" of unvegetated, shallow-water marine habitats. 1. distribution, abundance and primary production. *Estuaries*, 19(2A):186–201.

Mason, D., Amin, M., Davenport, I., Flather, R., Robinson, G., and Smith, J. (1999). Measurement of recent intertidal sediment transport in Morecambe Bay using the waterline method. 49:427–456.

Méléder, V., Barillé, L., Launeau, P., Carrère, V., and Rincé, Y. (2003). Spectrometric constraint in analysis of benthic diatom biomass using monospecific cultures. *Remote Sensing of Environment*, 88:386–400.

Méléder, V., Barillé, L., Rincé, Y., Morançais, M., Rosa, P., and Gaudin, P. (2005). Spatio-temporal changes in microphytobenthos structure analysed by pigment composition in a macrotidal flat (Bourgneuf Bay, France). *Marine Ecology Progress Series*, 297:83–99.

Middelburg, J. J., Barranguet, C., Boschker, H. T., Herman, P. M., Moens, T., and Heip, C. H. (2000). The fate of intertidal microphytobenthos carbon: An in situ C-13-labeling study. *Limnology and oceanography*, 45(6):1224–1234.

Migné, A., Spilmont, N., and Davoult, D. (2004). In situ measurements of benthic primary production during emersion: seasonal variations and annual production in the Bay of Somme (eastern English Channel, France). *Continental Shelf Research*, 24:1437–1449.

Miller, D. C., Geider, R. J., and MacIntyre, H. L. (1996). Microphytobenthos: The ecological role of the "secret garden" of unvegetated, shallow-water marine habitats. 2. role in sediment stability and shallow-water food webs. *Estuaries*, 19(2A):202–212.

Montani, S., Magni, P., and Abe, N. (2003). Seasonal and interannual patterns of intertidal microphytobenthos in combination with laboratory and areal production estimates. *Marine Ecology Progress Series*, 249:79–91.

Nicotri, M. (1977). Effects of four marine intertidal herbivores on the microflora. *Ecology*, 58(5):1020–1032.

Oh, S.-H. and Koh, C.-H. (1995). Distribution of diatoms in the surficial sediments of the Mangyung–Dongjin tidal flat, west coast of Korea (Eastern Yellow Sea). *Marine Biology*, 122:487–496.

Paterson, D. and Hagerthey, S. (2001). 5 microphytobenthos in contrasting coastal ecosystems: biology and dynamics. *Ecological comparisons of sedimentary shores*, pages 105–125.

Paterson, D. M., Wiltshire, K. H., Miles, A., Blackburn, J., Davidson, I., Yates, M. G., McGrorty, S., and Eastwood, J. A. (1998). Microbiological mediation of spectral reflectance from intertidal cohesive sediments. *Limnology and Oceanography*, 43(6):1207–1221.

Perkins, R. G., Underwood, G. J. C., Brotas, V., Snow, G. C., Jesus, B., and Ribeiro, L. (2001). Responses of microphytobenthos to light: primary production and carbohydrate allocation over an emersion period. *Marine Ecology Progress Series*, 223:101–112.

Pettorelli, N., Vik, J. O., Mysterud, A., Gaillard, J.-M., Tucker, C. J., and Stenseth, N. C. (2005). Using the satellite-derived NDVI to assess ecological responses to environmental change. *Trends in Ecology and Evolution*, 20(9):503–520.

Rebetez, M., Mayer, H., Dupont, O., Schindler, D., Gartner, K., Kropp, J. P., and Menzel, A. (2006). Heat and drought 2003 in Europe: a climate synthesis. *Ann. For. Sci.*, 63:569–577.

Riera, P. (2007). Trophic subsidies of *Crassostrea gigas*, *Mytilus edulis* and *Crepidula fornicata* in the Bay of Mont Saint Michel (France): A δ^{13}C and δ^{15}N investigation. *Estuarine, Coastal and Shelf Science*, 72:33–41.

Ruddick, K. G., Ovidio, F., and Rijkeboer, M. (2000). Atmospheric correction of SeaWiFS imagery for turbid coastal and inland waters. *Applied Optics*, 39(6):897–912.

Ryu, J.-H., Kim, C.-H., Lee, Y.-K., Won, J.-S., Chun, S.-S., and Lee, S. (2008). Detecting the intertidal morphologic change using satellite data. *Estuarine, coastal and shelf science*, 78:623–632.

Sabbe, K. (1993). Short-term fluctuations in benthic diatom numbers on an intertidal sandflat in the Westerschelde estuary (Zeeland; The Netherlands). *Hydrobiologia*, 269/270:275–284.

Serôdio, J., da Silva, J. M., and Catarino, F. (2001). Use of *in vivo* chlorophyll *a* fluorescence to quantify short-term variations in the productive biomass of intertidal microphytobenthos. *Marine Ecology Progress Series*, 218:45–61.

Seuront, L. and Leterme, C. (2006). Microscale patchiness in microphytobenthos distributions: evidence for a critical state. *Functioning of microphytobenthos in estuaries*, pages 167–185.

Shaffer, G. P. and Onuf, C. P. (1985). Reducing the error in estimating annual production of benthic microflora: hourly to monthly rates, patchiness in space and time. *Marine Ecology - Progress Series*, 26(3):221–231.

Siegel, D. A., Wang, M., Maritorena1, S., and Robinson, W. (2000). Atmospheric correction of satellite ocean color imagery: The black pixel assumption. *Applied Optics*, 39(21):3582–3591.

Smith, D. J. and Underwood, G. J. (1998). Exopolymer production by intertidal epipelic diatoms. *Limnology and Oceanography*, 43(7):1578–1591.

Smith, G., Thompson, A., Möller, I., and Kromkamp, J. (2003). Using hyperspectral imaging for the assesment of mudflat surface stability. *Journal of Coastal Research*, 20(0):000–000.

Spilmont, N., Davoult, D., and Migné, A. (2006). Benthic primary production during emersion: In situ measurements and potential primary production in the Seine Estuary (English Channel, France). *Marine Pollution Bulletin*, 53:49–55.

Stapel, J. and de Jong, D. (1998). *Ontwikkelingen in de biomassa van het microfytobenthos in de Oosterschelde en Westerschelde in de periode 1981–1996*. Rijksinstituut voor Kust en Zee.

Steven, M. D., Malthus, T. J., Baret, F., Xu, H., and Chopping, M. J. (2006). Intercalibration of vegetation indices from different sensor systems. *Remote Sensing of Environment*, 88:412–422.

Thornton, D. C., Dong, L. F., Underwood, G. J., and Nedwell, D. B. (2002). Factors affecting microphytobenthic biomass, species composition and production in the Colne Estuary (UK). *Aquatic Microbial Ecology*, 27:285–300.

Tolhurst, T., Black, K., Shayler, S., Mather, S., Black, I., Baker, K., and Paterson, D. (1999). Measuring the in situ erosion shear stress of intertidal sediments with the Cohesive Strength Meter (CSM). *Estuarine, coastal and shelf science*, 49(2):281–294.

Trites, M., Kaczmarska, I., Ehrman, J., Hicklin, P., and Ollerhead, J. (2005). Diatoms from two macro-tidal mudflats in Chignecto Bay, Upper Bay of Fundy, New Brunswick, Canada. *Hydrobiologia*, 544:299–319.

Underwood, G. J. (2002). Adaptations of tropical marine microphytobenthic assemblages along a gradient of light and nutrient availability in Suva Lagoon, Fiji. *Eur. J. Phycol.*, 37:449–462.

Underwood, G. J. C. and Kromkamp, J. (1999). Primary production by phytoplankton and microphytobenthos in estuaries. *Advances in Ecological Research*, 29:93–153.

Vilas, F., Arche, A., Ferrero, M., and Isla, F. (1999). Subantarctic macrotidal flats, cheniers and beaches in San Sebastian Bay, Tierra Del Fuego, Argentina. *Marine Geology*, 160:301–326.

Yallop, M. L., de Wilder, B., Paterson, D. M., and Stal, L. J. (1994). Comparative structure, primary production and biogenic stabilization of cohesive and non-cohesive marine-sediments inhabited by microphytobenthos. *Estuarine, coastal and shelf science*, 39(6):565–582.